DETERMINATION OF ELECTROSTATIC CHARGE DENSITY AND ADHESION FORCE OF PARTICLES ON A GLASS SURFACE USING AN ELECTROSTATIC DETACHMENT METHOD

An Undergraduate Research Scholars Thesis

by

HASSAN EJAZ HAIDER and MARYAM AL-BUAINAIN

Submitted to the Undergraduate Research Scholars program at
Texas A&M University
in partial fulfillment of the requirements for the designation as an

UNDERGRADUATE RESEARCH SCHOLAR

Approved by Research Advisor: Dr. Bing Guo

May 2020

Majors: Mechanical Engineering

TABLE OF CONTENTS

ABSTRACT

Determination of Electrostatic Charge Density and Adhesion Force of Particles on a Glass Surface Using an Electrostatic Detachment Method

Hassan Ejaz Haider and Maryam Al-Buainain
Department of Mechanical Engineering
Texas A&M University

Research Advisor: Dr. Bing Guo
Department of Mechanical Engineering
Texas A&M University

Attachment of particles to certain surfaces like glass plays a critical role in engineering and natural processes. An application can be found in the solar energy field as the accumulation of dust particles on the solar photovoltaic (PV) panel surface can reduce the efficiency of the solar panel with time. The main objective was to determine whether the electrostatic detachment method can be used to calculate electrostatic charge density and the upper limit of adhesion force of dust particles at various air humidity levels. The independent variables in this investigation were particle diameter and air humidity. The dependent variables were the electrostatic charge density and the upper limit of adhesion force between a particle and the glass surface. The apparatus used in the experiment included a microscope, a high-speed camera, a high voltage amplifier, a data acquisition system and ITO-coated glass plates housed in a 3D-printed chamber. Upon application of a steady uniform electric field, the particles traveled from the bottom glass plate to the top glass plate. The arrival of particles at the top glass plate was recorded using the high-speed camera at 4100 frames per second (fps) from which the time of flight was obtained. Using image analysis software, the particle size was extracted. The experiment was carried out at

relative humidity (RH) levels of 10%, 30%, and 80% at atmospheric pressure. The results showed that the upper limit of adhesion force increased with increasing particle diameters at all humidity levels; the highest adhesion force magnitudes were found at 30% RH. On the other hand, electrostatic charge density decreased with increasing particle size. Additional experiments are needed to obtain more statistically meaningful results.

ACKNOWLEDGMENTS

The authors of this paper are grateful for the guidance and support given to them by Dr. Bing Guo, Associate Professor in the Mechanical Engineering department at Texas A&M University at Qatar (TAMU-Q). The authors would also like to thank Dr. Wasim Javed, Research Scientist at TAMU-Q, who helped in setting up the experimental apparatus in the lab. Lastly, the authors thank Undergraduate Research Scholars program for giving us the opportunity to be part of the program.

NOMENCLATURE

F_{Ad}	Adhesion force
A_p	Projected area of particle
F_c	Coulomb force
DAQ	Data Acquisition
F_d	Drag force
E	Electric field
g	Gravitational acceleration
F_g	Gravitational force
HVA	High Voltage Amplifier
ITO	Indium Tin Oxide
PV	Photovoltaic
q	Particle charge
m_p	Particle mass
d	Equivalent diameter
τ	Relaxation time
t	Flight time
y	Travel distance between electrodes
V	Velocity
η	Viscosity of air
v	Voltage
RH	Relative Humidity

CHAPTER I

INTRODUCTION

Micrometer-sized particles like dust can accumulate on surfaces with the progress of time. Such accumulation can lead to corrosion if the dust was humid [1], or it can reduce the efficiency of a PV solar panel by reducing the area exposed to sunlight [2]. To automatically remove the dust from PV panels, advanced methods like the electrodynamic screen (EDS) are currently under development [3]. EDS method repels deposited dust on the PV panel. It depends on the electrostatic charge of the accumulated dust particles and the adhesion force between the particles and surface.

The main objective is to see whether electrostatic detachment method coupled with a high-speed camera and microscope can be used to determine electrostatic charge density and upper limit of adhesion force. If particle motion is observed and captured after applying the electric field, another objective is to identify any trends of how electrostatic charge density and upper limit of adhesion force vary with particle size and air humidity levels.

CHAPTER II

METHODS

In this research, the upper limit of adhesion force and electrostatic charge density between dust particles of different sizes and ITO glass plates were calculated. This section is split into two sections experimental and data analysis. The experimental section details experiment design, and data analysis section outlines the process followed to calculate upper limit of adhesion force and electrostatic charge density.

Experimental

The apparatus consisted of a microscope, transparent glass plates coated with ITO on one side, chamber to house the plates, High-Voltage Amplifier (HVA), DAQ board, high-speed camera, and computer. The schematic in Figure 1 shows the experimental setup along with how the components were connected.

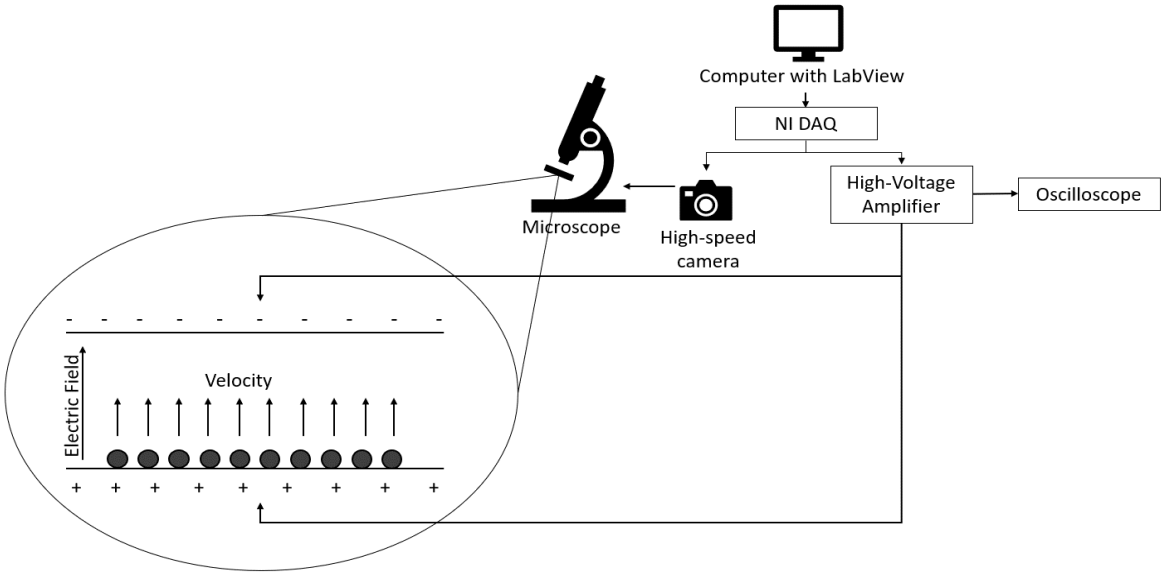

Figure 1. Schematic of the experimental setup.

The real-life experimental setup organized in the research lab is shown in Figure 2. The figure is labelled to show the individual components of the setup following from Figure 1.

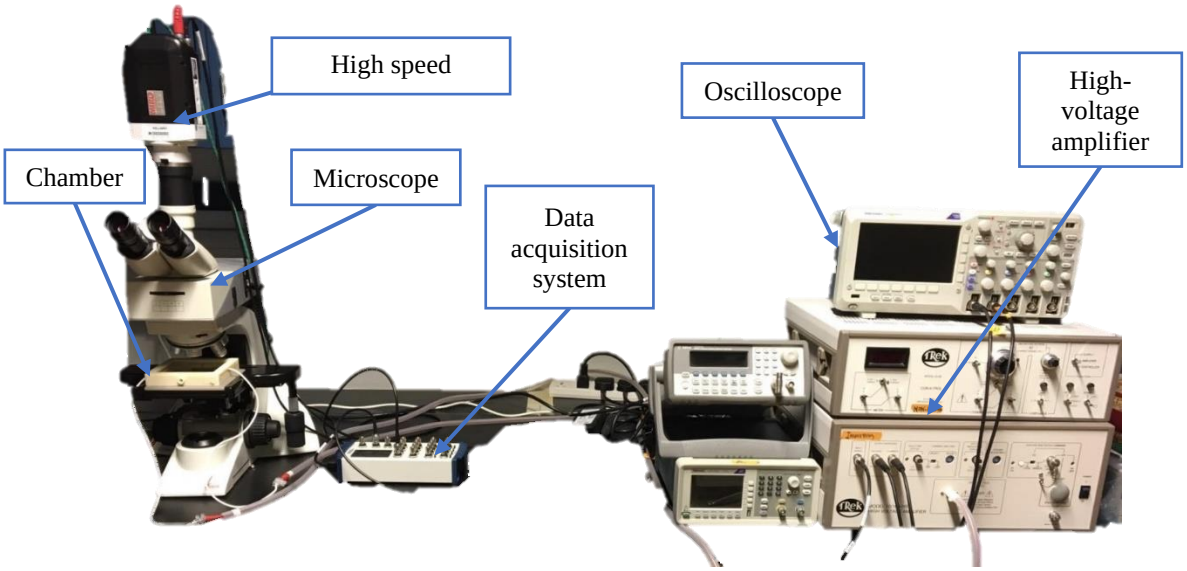

Figure 2. Real-life experimental setup.

The need for LabVIEW software was identified after preliminary tests were performed. During preliminary testing, the high-speed camera was triggered manually from the software installed on the computer. After the camera started recording, the high-voltage amplifier was turned on to apply the electric field across the glass plates. At this point, it was realized that in order to reduce this time gap to reduce data loss, the camera and voltage supply need be triggered at the same time. This was done using LabVIEW which sends a signal to a DAQ board to trigger the camera and voltage supply in sync. The oscilloscope was used to observe signal generation during the duration of the experiment. The procedure for the experiment is as follows:

1. Dust particles were deposited on the bottom transparent glass plate housed in the chamber. The dust was poured through a mesh to deposit particles of less than 70 µm on the glass plate. The chamber was designed, and 3D printed, an image is shown in Figure 3 below.

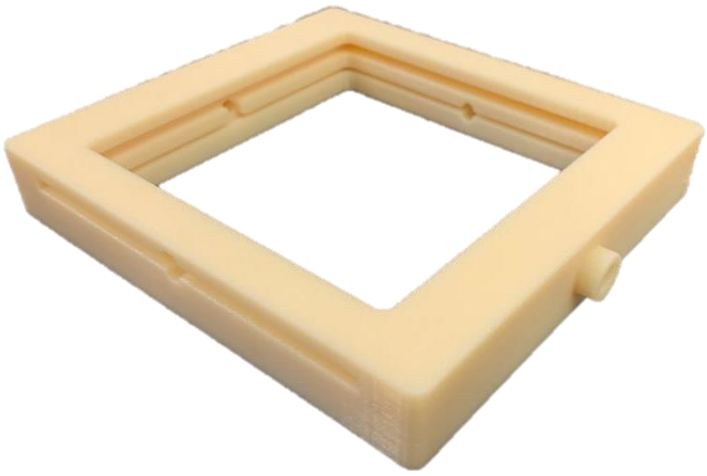

Figure 3. Photo of housing chamber.

2. The high-speed camera attached to the microscope was used to take a single image of the lower plate after which it was focused on the upper plate.
3. Computer with LabVIEW was used to generate a signal of known amplitude to send to the DAQ to trigger the camera and voltage supply at the same time.
4. After triggering, the camera takes continuous images based on the specified frame rate, in this case 4100 fps, when the high voltage is applied.
5. The plates were wiped cleaned using tissue and brush to remove residue of particles from previous runs.
6. Captured frames were analyzed using ImageJ to determine particle area. The data from ImageJ was then transferred to MS Excel software for further data analysis and graph generation.

Image analysis and calculations

Figure 4 shows a sample image of the of the top plate taken by the high-speed camera after running the experiment. The camera was set to take images at 4100 fps for 2.716 seconds.

The particles encircled in red are an example of the size of the particles that were considered for further analysis.

Figure 4. Sample image taken from high-speed camera.

This image was then exported to ImageJ where it was processed to measure particle area. Figure 5 shows an example of the image when exported to ImageJ after background subtraction.

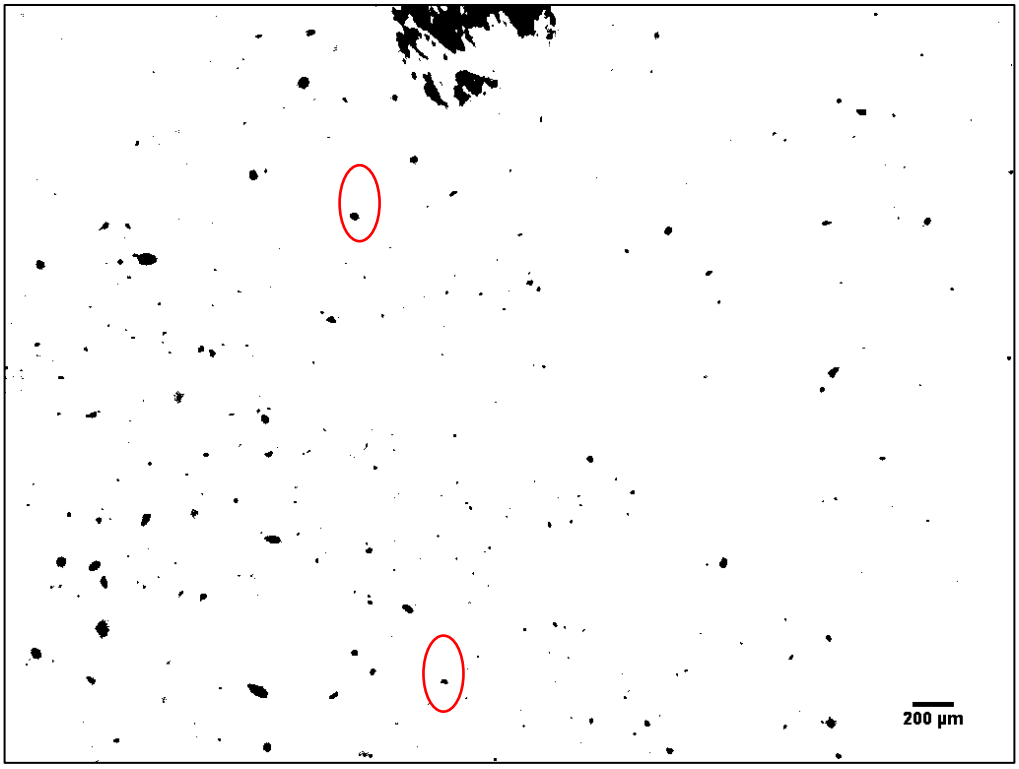

Figure 5. Sample of image processing on ImageJ.

ImageJ calculates the particle area from which the equivalent particle diameters were obtained using Equation 1 in mm^2.

$$A_p = \frac{1}{6}\pi d^3 \quad (1)$$

The flight time of the particles in seconds was calculated based on the settling frame number. The video taken by the high-speed camera was split into individual frames. Individual particles were followed as they arrived at the top plate until the frame where the particle finally settled was identified. This settling frame, which was number for example 10/4100 frames, was used to calculate time of flight using Equation 2.

$$t_{flight} = \frac{1}{4100\ fps} settling\ frame\ number \quad (2)$$

A free body diagram of the particle in motion is shown in Figure 6. It shows the three forces that act on the particle in steady state; Coulomb force (F_c) which the particle is subjected

to due to the electrical field, drag force (F_D) due to the surrounding atmosphere and gravitational force (F_g) exerted by the earth's gravitational field.

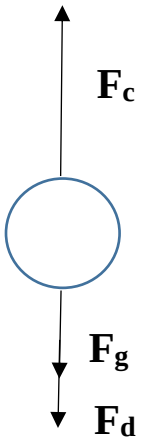

Figure 6. Free body diagram of the particle while flying.

The particle motion when in steady-state flight are described by Equation 3. In Equation 3, Coulomb force and gravitational forces are constants whereas drag force changes for individual particles as particle diameter and terminal velocity is varied.

$$F_c - F_D - F_g = 0 \ (3)$$

Equations 4, 5 and 6 give the Coulomb, drag force and gravitational force taken from literature [4].

$$F_c = Eq \ (4)$$

$$F_D = 3\pi\eta V d \ (5)$$

$$F_g = \frac{\pi d^3 \rho}{6} g \ (6)$$

Initially the particle accelerates for a short period of time. Therefore, the drag force acting on the particle will increase as it accelerates. To be able to assume that particles accelerate for a negligible time, another quantity known as relaxation time was calculated using Equation 7.

$$\tau = \frac{\rho d^2 g}{18\eta} \ (7)$$

After calculating the relaxation time, the particles were screened and only those particles were further analyzed which had a ratio of less than 5% of relaxation time to the total flight time. This showed that majority of the particle motion was in steady state, therefore, Equation 4 could be applied. The travel distance of the particles was taken to be the distance between the two glass plates which was 5.3 mm. Using the travel distance (y), flight time given by Equation 2 and relaxation time given by Equation 7, the terminal velocity of the particles was calculated using Equation 8 in m/s [4].

$$V = \frac{y}{t_{flight} - \tau(1 - e^{-\frac{t_{flight}}{\tau}})} \quad (8)$$

For particles that pass the 5% threshold, their upper limit of adhesion force was calculated using Equation 9.

$$F_{Ad} \leq F_c - F_g \quad (9)$$

The adhesion force is the upper limit of the contact force between the particle and the surface that needs to be overcome for the particle to take flight. At this point, the drag force is zero, hence, adhesion force is the difference between the Coulomb force and gravitational force acting in the opposite direction. The electrostatic charge of the particle was calculated using Equation 5, and charge density was calculated by dividing the electric charge with particle area. The value of electric field (E) in Equation 4 was calculated by dividing the potential across the plate with the distance between the plates as this is a uniform electric field.

After performing the preceding analysis for several particles on MS Excel, a scatter chart was plotted to show the distribution of charge density and upper limit of adhesion force as a function of particle diameter. The voltage supply was set to 8 kV for all experiments. The air humidity was set at various levels, and experiments were performed for 10%, 30%, and 80% relative humidity (RH).

CHAPTER III

RESULTS AND DISCUSSION

Electrostatic charge density results for RH values of 10%, 30%, and 80% are shown in Figure 7. These values were analyzed under a constant applied voltage of 8 kV.

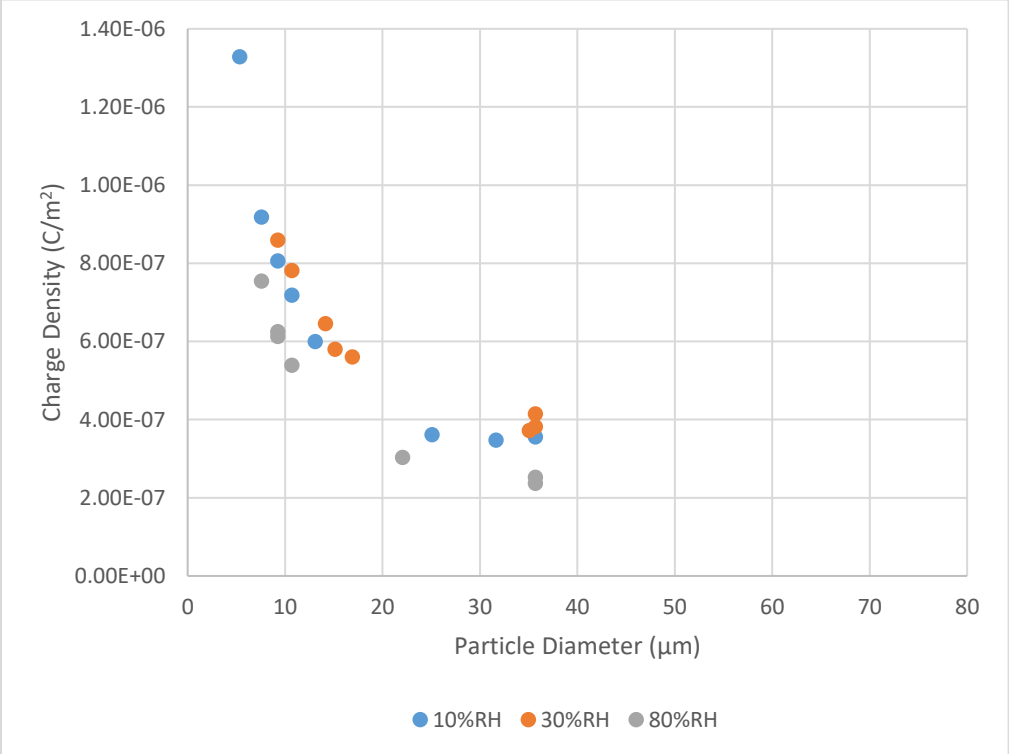

Figure 7. Charge density versus particle diameter.

The electrostatic charge density of the particles shows a decreasing trend from 5 µm to 40 µm particle diameter. It can be observed that the highest charge density value was for particles exposed to 30% RH, followed by 10%, and 80% RH in that order. The upper limit of adhesion

force for the same above-mentioned particles at the various relative humidity levels is shown in Figure 8.

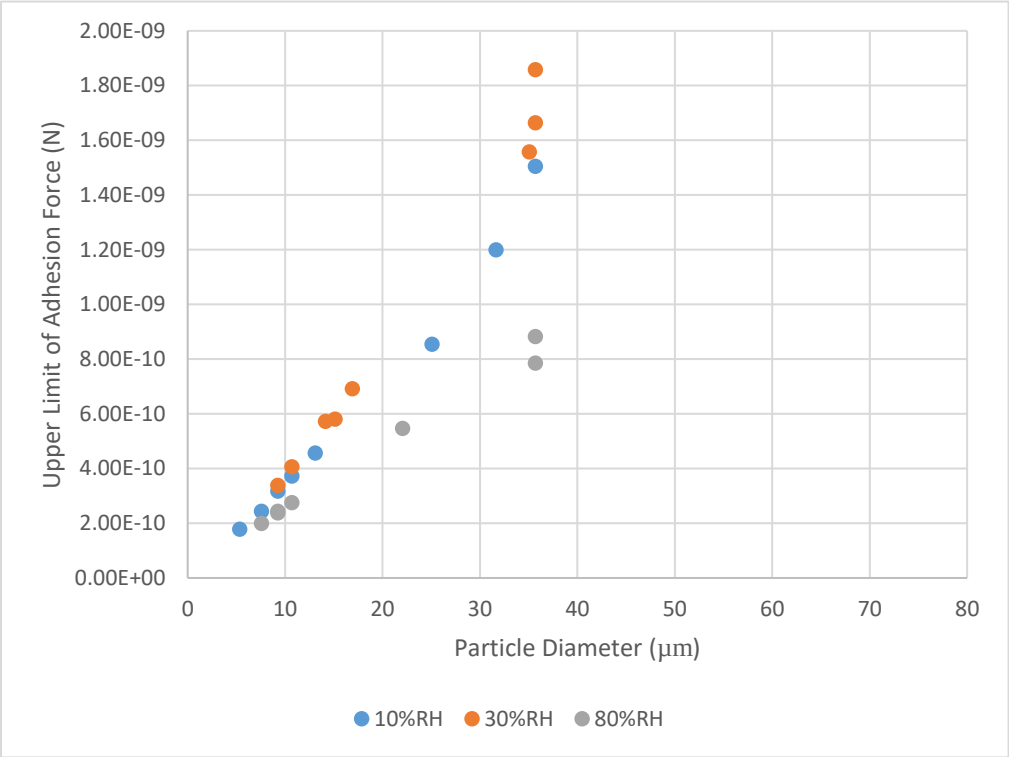

Figure 8. Upper limit of adhesion force versus particle diameter.

It can be noticed that the adhesion force has a positive correlation with particle diameter. The increasing trend has also been observed in literature. One study measured adhesion force of particles on a surface using a centrifugal technique. The results showed that for different materials, such as phosphate rock and limestone, and particle diameters, the adhesion force increased as particle diameter increased non-linearly [5]. In this experiment, the adhesion force for varying particle diameters was calculated at different air humidity levels. Like charge density the highest adhesion force was observed at 30% RH, followed by 10% RH, and 80% RH in that order. The results show that adhesion force is also dependent on air humidity and particle diameter.

To understand why such trends are observed, a deeper insight into how the particle composition of sand dust analyzed in these experiments affect charge density and adhesion force is required. At 10% RH the particles are the driest in this experiment since concentration of water vapor in the environment is low. This means that moist air surrounding individual particles will not be as concentrated resulting in particles retaining their charge until they reach the upper plate. Likewise, at 80% relative humidity, the concentration of water vapor surrounding the particle increases. Since water is a good conductor of electrical charge, the particles lose their charge at a higher rate than at 10% relative humidity. This is reflected on Figure 7 as the graph shifts downwards as humidity levels rise. Therefore, electrostatic charge density and adhesion force are dependent on humidity. Higher humidity leads to better surface conductance resulting in a faster dissipation of electrostatic charge on the surface. This is consistent with the results obtained when electrostatic charge density decreases from at 80% RH. The graphs of 10% RH and 30% RH are intertwined whereas 10% RH should have displayed the largest magnitudes for electrostatic charge densities. One of the reasons is that it is assumed electrostatic charge density is constant, therefore, the expected trend was mentioned as before. However, at a fixed particle size, there is a distribution of charge, hence, the mixing in results at 10% RH and 30 % RH is observed. Secondly, not enough data was collected due to the small sample size data set. Further experiments need to be performed to obtain a better understanding of the trends showed for electrostatic charge density and upper limit of adhesion force. Third reason could be experimental uncertainty in keeping the humidity level constant while running the experiment.

Moreover, there is higher spread in the distribution of the particles from 20 μm to 40 μm, while a narrow spread is observed when the particle diameter is less than 20 μm. This can be due to various reasons including the effect of the distribution of Coulomb force and Van der Waals

forces with different particle size at different rates. Secondly, the variation can be due to the sand dust, having differences in material composition. This would result in a distribution of electrostatic charge densities and adhesion forces at a fixed particle diameter. This dependency of particle charge on material composition was also found in literature. The findings of a study showed that level of charging and polarity is dependent on material composition of particles [6]. In addition, Figure 7 and 8 show that there are some particles that are not accounted for. The unaccounted particles are those that did not take flight when the electric field was applied. For these particles, the Coulomb force is less than the adhesion force due to which they did not take flight. In addition, there might be some particles that are positively charged, thus, those particles that had the same polarity as the applied electric field are not accounted for. Therefore, experimental design limitations did not allow for all particles in the sample dust to be analyzed.

CHAPTER IV

CONCLUSION

The results show that electrostatic detachment method coupled with a high-speed camera and microscope can be used to capture particle motion which allowed for trends of upper limit of adhesion force and electrostatic charge density to be identified. At different air humidity levels, the magnitudes of upper limit of adhesion force and electrostatic charge density varied. The electrostatic charge density of sand dust decreased as particle diameter increased. The adhesion force between particles of sand dust and glass plates displayed a positive correlation with increasing particle diameter. Both parameters increased at 30% RH and decreased at 80% RH with 10 % RH lying in between. The trend displayed at all humidity levels was similar showing that upper limit of particle adhesion force and electrostatic charge density is dependent on air humidity as well as particle size.

Due to the unfortunate circumstances surrounding the COVID-19 pandemic, the initial research plan for experimental activities was not completed. This did not allow us to redo any experiments or perform further data acquisition and analysis. Therefore, once situation permits, future research work will include performing further experiments to get statistically meaningful results. Moreover, particle composition analysis will be performed to get a more accurate description of the sample dust used in the experiments. In addition, future work can also include investigating the effects of changing surface and particle material along with air humidity to see how surface properties and particle composition affect the upper limit of adhesion force and electrostatic charge density.

REFERENCES

[1] Xue-Yan Lin and Ji-Gao Zhang, "Dust corrosion," Proceedings of the 50th IEEE Holm Conference on Electrical Contacts and the 22nd International Conference on Electrical Contacts Electrical Contacts, 2004., Seattle, WA, USA, 2004, pp. 255-262.

[2] B. R. Paudyal and S. R. Shakya, "Dust accumulation effects on efficiency of solar PV modules for off grid purpose: A case study of Kathmandu," *Solar Energy*, vol. 135, pp. 103–110, 2016.

[3] C.-Y. Chen, J. K. Chesnutt, C.-H. Chien, B. Guo, and C.-Y. Wu, "Dust removal from solar concentrators using an electrodynamic screen," Solar Energy, vol. 187, pp. 341–351, 2019.

[4] W. C. Hinds, Aerosol technology. New York: J. Wiley, 1982.

[5] M. A. Felicetti, F. Piantino, J. R. Coury, and M. L. Aguiar, "Influence of removal time and particle size on the particle substrate adhesion force," *Brazilian Journal of Chemical Engineering*, vol. 25, no. 1, pp. 71–82, 2008.

[6] Rodrigues, M. V., Jr., W. D. M., Almeida, R. G., & Coury, J. R. (2006). Measurement of the electrostatic charge in airborne particles: II - particle charge distribution of different aerosols. Brazilian Journal of Chemical Engineering, 23(1), 125–133. doi: 10.1590/s0104-66322006000100014